



# Modification of Non-Activated Carbon from Rubber Fruit Shells with 3-(Aminopropyl)-Triethoxysilane and Its Adsorption Study on Coomassie Brilliant Blue and Methylene Blue in Solution

Buhani · Jilda Sofiana Dewi ·  
Nadya Syarifatul Fajriyah · Mita Rilyanti ·  
Suharso · Sumadi · Khalid Z. Elwakeel

Received: 7 February 2023 / Accepted: 6 July 2023 / Published online: 23 August 2023  
© The Author(s), under exclusive licence to Springer Nature Switzerland AG 2023

**Abstract** This study involved modifying carbon derived from rubber fruit shells, referred to as nAC-RFs, without activation. The modification process utilized a silane agent known as 3-Aminopropyl-Triethoxysilane (APTES), resulting in the formation of nAC-RFs-S. To confirm the successful modification, the adsorbent underwent characterization using an Infrared Spectrometer (IR) to identify functional groups and Scanning Electron Microscopy-Energy Dispersive-X-ray (SEM-EDX) to analyze surface morphology and constituent elements. The adsorption capacity of nAC-RFs-S was evaluated through batch adsorption experiments involving Coomassie Brilliant

Blue (CBB) dye (anionic) and Methylene Blue (MB) dye (cationic). The optimal conditions for CBB and MB adsorption on both nAC-RFs and nAC-RFs-S were found to be pH 5, a contact time of 90 min, and a temperature of 27 °C. The adsorption kinetics of CBB and MB onto nAC-RFs and nAC-RFs-S followed the pseudo-second-order kinetic model. The pseudo-second-order rate constants ( $k_2$ ) for CBB were  $2.674 \times 10^{-3}$  and  $0.185 \times 10^{-3}$  (g/mg·min) for nAC-RFs and nAC-RFs-S, respectively, while for MB, the corresponding values were  $2.735 \times 10^{-3}$  and  $0.415 \times 10^{-3}$  (g/mg·min). CBB adsorption tended to conform to the Freundlich adsorption isotherm model on nAC-RFs, whereas, on nAC-RFs-S, it tended to align with the Langmuir adsorption isotherm model. For MB, both nAC-RFs and nAC-RFs-S exhibited adsorption tendencies that followed the Freundlich isotherm model. The nAC-RFs-S adsorbent demonstrated remarkable effectiveness in adsorbing CBB and MB in solution, with the ability to be reused for up to three cycles while maintaining an adsorption percentage exceeding 80%. Consequently, the nAC-RFs-S adsorbent holds promise as an advantageous and efficient solution for combating water pollution caused by toxic chemicals like synthetic dyes.

Buhani · J. S. Dewi · N. S. Fajriyah · M. Rilyanti · Suharso  
Department of Chemistry, Faculty of Mathematic  
and Natural Sciences, University of Lampung,  
Bandar Lampung 35145, Indonesia  
e-mail: buhani\_s@yahoo.co.id

Sumadi  
Department of Electrical Engineering, Faculty  
of Engineering, University of Lampung,  
Bandar Lampung 35145, Indonesia

K. Z. Elwakeel (✉)  
Environmental Chemistry Division, Environmental  
Science Department, Faculty of Science, Port Said  
University, Port Said, Egypt  
e-mail: khalid\_elwakeel@sci.psu.edu.eg

K. Z. Elwakeel  
College of Science, Department of Chemistry, University  
of Jeddah, Jeddah, Saudi Arabia

**Keywords** Adsorption–desorption · Carbon  
modification · Silane agents · Coomassie brilliant  
blue · Methylene blue

## 1 Introduction

Over the past few decades, the use of water and hazardous chemicals has increased due to industrialization, urbanization, and agricultural expansion. This rapid expansion has had negative consequences for the environment, particularly in terms of water pollution (Bhavyasree & Xavier, 2021; Moosavi et al., 2020). Among the industries contributing to water pollution, the textile industry stands out (Iwuozor et al., 2021). It has a harmful impact on the environment primarily because of the waste generated, specifically the waste from synthetic dyes. Statistics indicate that the textile industry consumes an estimated 60% of the total dye production, with approximately 10–15% of these dyes ending up as waste (Çelekli & Bozkurt, 2013). Even at very low concentrations, the presence of dyes in water can impede the penetration of light into the water's surface, disrupting the photosynthesis of aquatic plants. Additionally, many of these dyes possess carcinogenic, mutagenic, teratogenic, and toxic properties, posing risks to humans, fish, and microorganisms (Abdel-ghani et al., 2017).

Coomassie Brilliant Blue (CBB/C<sub>45</sub>H<sub>44</sub>N<sub>3</sub>NaO<sub>7</sub>S<sub>2</sub>) and Methylene Blue (MB/C<sub>16</sub>H<sub>18</sub>N<sub>3</sub>SCl) are widely used dyes. CBB dye, which falls under the category of triphenylmethane dyes, has the potential to cause mutagenic and teratogenic effects on living organisms (Ibrahim et al., 2019; Priya et al., 2018). Exposure to CBB can lead to irritation in the eyes and digestive tract of living organisms (Thamer et al., 2019). Moreover, if CBB dye persists in the environment for an extended period, it can transform into a non-degradable and toxic organic pollutant (Abdel-Ghani et al., 2017). Another commonly employed dye in the industrial sector is methylene blue (MB) due to its favorable solubility. MB dye, an aniline-based dye, can have detrimental effects on microorganisms, animals, and humans, thereby contributing to environmental pollution. These adverse effects can be attributed to the complex and aromatically structured nature of MB dye, making it challenging to degrade (Jamwal et al., 2017). Given the negative consequences of uncontrolled dispersion of dyes in the environment, particularly in water bodies, it is crucial to implement measures for treating dye waste before its disposal into the environment.

Currently, a range of methods has been developed to mitigate pollution stemming from liquid waste,

including physicochemical techniques like coagulation/flocculation, membrane separation, ion exchange, chemical oxidation, electrochemical processes, adsorption, and photocatalysis. These methods have been employed to eliminate dyes and metal ions from wastewater (Wong et al., 2016; Kanakaraju et al., 2017; Buhani et al., 2019; Katheresan et al., 2018; Elgarahy et al., 2021; Al-Hazmi et al., 2022; Annisa et al., 2022). Among these diverse approaches, adsorption methods are frequently utilized to treat liquid waste that contains toxic dyes (Buhani et al., 2019; Elwakeel et al., 2020). This preference is due to the simplicity, cost-effectiveness, and environmentally friendly nature of adsorption methods (Buhani et al., 2017; Elgarahy et al., 2019). Typically, the adsorption process employs adsorbents, which can be either synthesized or modified natural materials.

The effectiveness of using adsorption methods to treat dye wastewater relies heavily on the choice of adsorbent. Carbon is a natural and efficient adsorbent for removing pollutants originating from dyes. It can be derived from various carbon-rich sources, including plants containing lignin, like rubber fruit shells, which have a lignin content of 33.54%. As a result, rubber fruit shells hold significant potential for conversion into carbon with excellent adsorption capacity (Buhani et al., 2023; Zulaicha et al., 2022). However, the binding capability of carbon for these dye compounds is limited due to certain drawbacks. These include the relatively ineffective separation of the adsorbent from the filtrate during filtration and the lengthy centrifugation time required in the adsorption process (Rocha et al., 2020).

Enhancing carbon quality can be accomplished by activating it physically or chemically to produce activated carbon. However, the activation process is time-consuming and expensive. Therefore, in this research, the quality improvement of carbon derived from rubber fruit shells (nAC-RFs) was pursued without activation through an increased number of active sites using the silanization process. The aim of the silanization process, utilizing organosilane compounds like 3-Aminopropyl triethoxysilane (APTES) (Wong et al., 2015), is to introduce functional groups as active adsorption sites.

Organosilane compounds act as coupling agents due to possessing two distinct active groups that are bonded to silica atoms within the molecule, thereby establishing chemical bonds between organic and

inorganic materials (Huang & Hu, 2008). The APTES compound can generate silanol and siloxane groups, which are expected to enhance the adsorption capacity of non-activated carbon toward dyes (Liu et al., 2013). The  $-NH_2$  functional group in APTES offers a significant opportunity for connecting with other target molecules (Can et al., 2009). Additionally, the APTES compound exhibits two types of active groups that enable it to react with compounds having anionic, cationic, or neutral properties (Munguía-Cortés et al., 2017).

In this investigation, the modification of carbon derived from rubber fruit shells without activation (nAC-RFs) was achieved by utilizing a silanization agent derived from the APTES compound, resulting in the development of an adsorbent and nAC-RFs-S for the adsorption of CBB and MB dyes. Parameters such as kinetics, adsorption isotherms, and the reusability of nAC-RFs-S were employed to evaluate the effectiveness of the adsorbent in capturing both cationic and anionic dyes, allowing for the practical implementation of the adsorbent in addressing and mitigating the dispersion of toxic dyes, particularly in aquatic environments.

## 2 Materials and Methods

### 2.1 Materials

The study utilized carbon sourced from rubber fruit shells acquired from rubber plantations located in East Lampung Regency, Indonesia. Chemical substances including coomassie brilliant blue (CBB), methylene blue (MB), 3-Aminopropyl triethoxysilane (APTES), HCl, NaOH, toluene, buffer solution, and ethanol were procured from the European Pharmacopoeia.  $KNO_3$  was also sourced from the European Pharmacopoeia.

### 2.2 The Production of Non-Activated Carbon (nAC-RFs) from Rubber Fruit Shells

The process begins with washing the rubber fruit shells and allowing them to dry under sunlight. Afterward, the shells are combusted inside an iron drum for around 6 h to generate carbon derived from the rubber fruit shells. Subsequently, the resulting carbon is finely crushed and filtered through a 100  $\mu m$  mesh sieve (nAC-RFs).

### 2.3 Modification of nAC-RFs with APTES

The method for preparing nAC-RFs-S is based on the procedure described by Shirendev et al., 2021. Initially, 25 g of nAC-RFs was combined with a 250 mL solution of APTES (30% (vol) in toluene) and agitated for 3 h at 50 °C. Subsequently, the mixture was filtered, and the solid residue was washed with deionized water until it attains a neutral pH. The solid material was then dried in an oven at 110 °C for 4 h, yielding nAC-RFs-S as the final product.

### 2.4 Characterization

To analyze the functional groups, the nAC-RFs, and nAC-RFs-S samples were subjected to characterization using an FTIR spectrometer (Prestige-21 Shimadzu, Japan). The surface morphology and constituent elements were observed and identified by employing SEM-EDX (Zeiss MA10, SEM-EDX, Gottingen, Germany).

### 2.5 Determination of Zeta Potential Value

0.1 g of both nAC-RFs and nAC-RFs-S were added to a flask containing 20 mL of 0.1 M  $NaNO_3$  solution. Following that, the starting pH was adjusted within the range of 3 to 12 by using 0.1 M HCl solution for acidic conditions and 0.1 M NaOH solution for basic conditions. The solution was then stirred using a stirrer for 24 h. Subsequently, the resulting pH was observed and measured using a pH meter.

### 2.6 Adsorption by Batch Method

All adsorption procedures were carried out using the batch method. The adsorbent and adsorbate were mixed using a shaker (Stuart SSL1-OB—Shaker, Orbital, Lab Scale, 230 V) at a speed of 150 rpm. The primary experiment aimed to examine the impact of initial pH ( $pH_0$ ) within the range of 3.0—11.0. The initial pH was adjusted by adding either a 0.10 mol/L HCl or NaOH solution to the dye solution with an initial concentration ( $C_0$ ) of 10 mg/L and an adsorbent mass of 0.1 g at a temperature of 27 °C. The second experiment sought to investigate the influence of different contact times ranging from 0 to 150 min using a dye solution volume ( $V$ ) of 0.025 L and  $C_0$  of 10 mg/L at 27 °C. Subsequently, an adsorption isotherm study was conducted similar to

the kinetic procedure, but with varying sample concentrations from 0 to 300 mg/L at 27 °C. The effect of similar ions was also explored by interacting with a mixture of CBB dye solution, nitrate anion, and phosphate at concentrations of 0.1, 0.25, and 0.35 mmol/L, respectively. The adsorption process was carried out under specific conditions (pH<sub>0</sub>: 5.0; V: 0.025 L; t: 90 min; T: 27 ± 1 °C; agitation speed: 150 rpm; adsorbent mass: 0.1 g). In each experiment, the filtrate or residual dye solution was analyzed to determine its concentration using a spectrophotometer at respective wavelengths (λ) of 558.0, 664, 201, and 719 nm (Agilent Cary 100).

All adsorption experiments were repeated three times. The quantity of adsorbed dye ( $q_t$ ) at time  $t$  (min) and equilibrium ( $q_e$ ) were determined using Eqs. 1 and 2, while the percentage of adsorbed dye was calculated using Eq. 3.

$$q_t = \frac{V}{W}(C_0 - C_t) \quad (1)$$

$$q_e = \frac{V}{W}(C_0 - C_e) \quad (2)$$

$$\text{Adsorption (\%)} = \frac{(C_0 - C_e)}{C_0} \times 100 \quad (3)$$

## 2.7 Reuse of Adsorbents

0.5 g of nAC-RFs-S was placed in a reaction tube. Afterward, 125 mL of either CBB or MB solution was added following specific conditions ( $C_0$ : 300 mg/L; pH<sub>0</sub>: 5.0;  $t$ : 90 min;  $T$ : 27 ± 1 °C; agitation speed: 150 rpm). The CBB or MB adsorbate was subsequently desorbed using a 40% ethanol solution. The resulting filtrate and precipitate were separated, and the precipitate was washed with water until it reaches a neutral pH. It was then dried in an oven at 40 °C for 3 h. The adsorbent can be reused for the adsorption of CBB or MB dye for up to 5 repeated cycles.

## 3 Results and Discussion

### 3.1 Adsorbent Modification and Characterization

Figure 1 illustrates the procedure for transforming rubber fruit shells into nAC-RFs-S. Before executing

the process outlined in Fig. 1, the acquired rubber fruit shells undergo a thorough rinse with running water to eliminate any impurities. Subsequently, the cleansed rubber fruit shells were sun-dried to reduce their moisture content. The next step involved carbonizing the rubber fruit shells in an iron drum for a duration of 6 h. The resulting carbon from the carbonization process retains a sizable particle size and must therefore be finely pulverized to yield nAC-RFs. Afterward, APTES was employed to modify the nAC-RFs via a silanization process.

In general, the process of silanization of nAC-RFs using APTES typically involves the hydrolysis of triethoxyl groups to form trihydroxyl groups, followed by the polycondensation of hydroxyl groups on the surface of nAC-RFs. Additionally, there are several potential reactions, including the interaction between silanol groups and hydroxyl groups after hydrolysis, resulting in the silanization of the nAC-RFs surface and the formation of nAC-RFs-S (Lee et al., 2004; Sahoo et al., 2021; Buhani et al., 2023).

Figures 2a and c demonstrate that both nAC-RFs and nAC-RFs-S display wide peaks in the wavenumber range of 3200–3600 cm<sup>-1</sup>, with a distinct peak at 3449 cm<sup>-1</sup>, indicating the presence of -OH groups. Furthermore, an absorption band is observed in the vicinity of 2368 cm<sup>-1</sup>, signifying the vibration of alkyl (C-H) groups. This observation is reinforced by peaks within the wavenumber range of 860–600 cm<sup>-1</sup>, specifically at 756 cm<sup>-1</sup> for nAC-RFs and 725 cm<sup>-1</sup> for nAC-RFs-S, indicating the existence of C-H bonds in both adsorbents. Additionally, there are absorption bands at wavenumbers 1620 cm<sup>-1</sup> for nAC-RFs and 1627 cm<sup>-1</sup> for nAC-RFs-S, indicating the presence of carboxylate groups (Martínez et al., 2006). In nAC-RFs-S (Fig. 2c), a peak at wavenumber 1527 cm<sup>-1</sup> suggests the presence of N-H groups (Kosa et al., 2012; Radoičić et al., 2010), and a peak at wavenumber 1126 cm<sup>-1</sup> is associated with the Si-O-C bond from APTES as a modifying agent (Fig. 2b) (Ahmad et al., 2017).

Figure 3 illustrates the surface characteristics and elemental composition of both nAC-RFs and nAC-RFs-S. In the case of nAC-RFs (Fig. 3a), the surface morphology reveals evenly distributed and uniform pores, along with pores of different sizes. However, upon modification with APTES, nAC-RFs-S (Fig. 3b) undergoes a reduction in surface porosity. This decrease is attributed to the binding

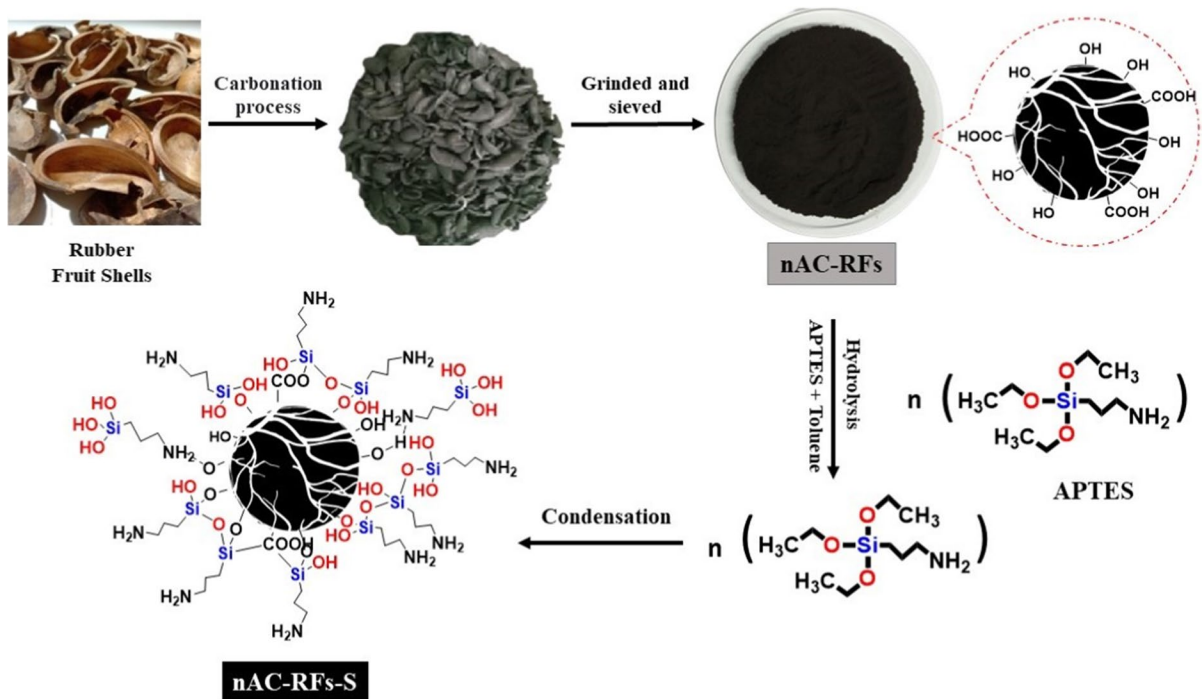


**Fig. 1** The scheme for modifying nAC-RFs into nAC-RFs-S

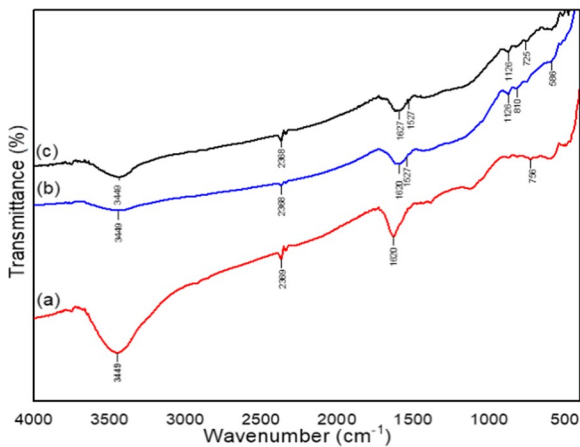


**Fig. 2** FTIR spectra of (a) nAC-RFs, (b) APTES, (c) and nAC-RFs-S

of APTES to the carbon pores, which fills them with functional groups derived from APTES (Shirendev et al., 2021). Consequently, these alterations can influence the enhancement of adsorption capacity through the presence of functional groups on the adsorbent’s surface. The occurrence of the silane

agent’s modification on nAC-RFs is supported by the EDX data presented in Fig. 3d, demonstrating the presence of diffraction peaks for nitrogen (N) and silicon (Si) elements originating from APTES, in addition to the carbon (C) and oxygen (O) elements found in nAC-RFs (Fig. 3c).

### 3.2 The $\text{pH}_{\text{PZC}}$ Value of the Adsorbent

Determination of the value of  $\text{pH}_{\text{PZC}}$  aims to determine the effect of pH on the surface charge of the adsorbent. The  $\text{pH}_{\text{PZC}}$  value is obtained from the exact value that crosses the zero point on the resulting graph of the value between the initial pH and the difference between the initial pH and the final pH (Ai et al, 2011). The adsorbent surface charge will be negative at  $\text{pH} > \text{pH}_{\text{PZC}}$  and positively charged at  $\text{pH} < \text{pH}_{\text{PZC}}$ . In this study, the  $\text{pH}_{\text{PZC}}$  values were obtained for nAC-RFs and nAC-RFs-S which exactly cut the zero point on the results graph. The value between the initial pH and the difference between the initial pH and the final pH was pH 7.09 and 9.02, respectively (Fig. 4).

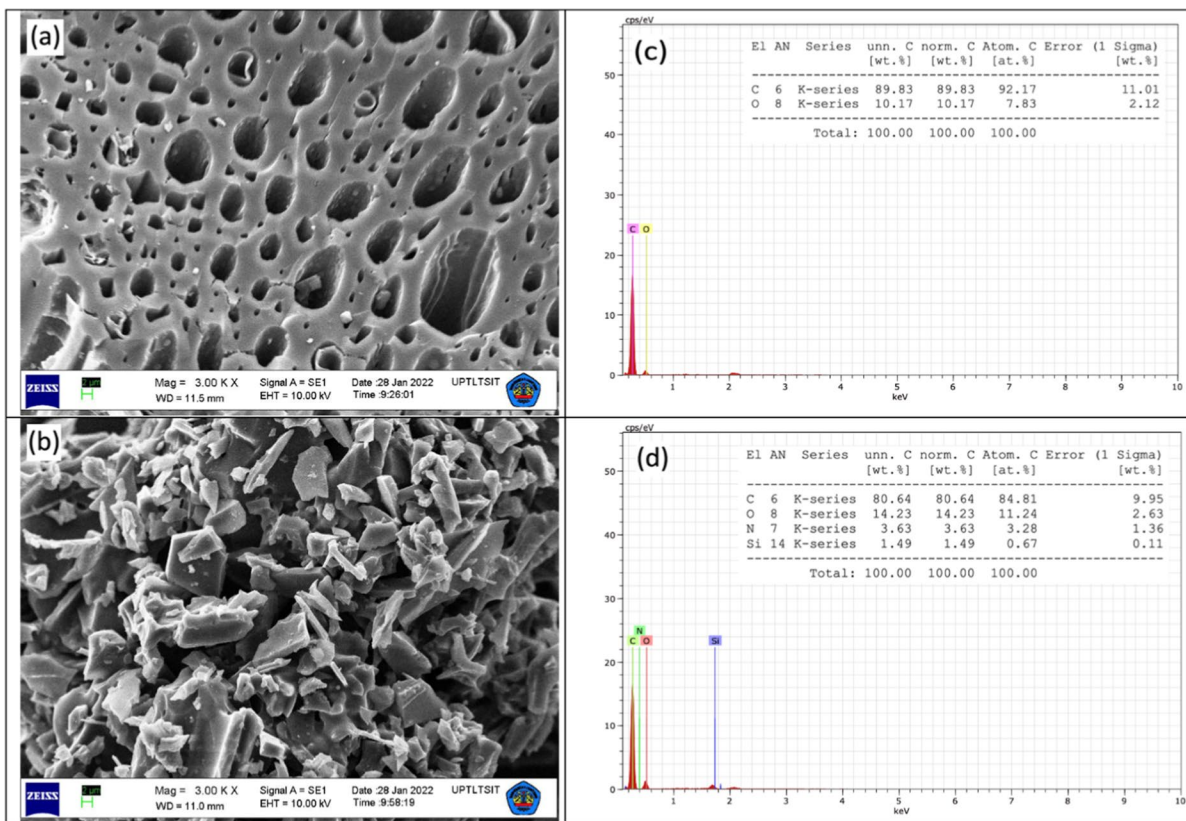


**Fig. 3** SEM–EDX (a, c) nAC-RFs and (b, d) nAC-RFs-S

### 3.3 Effect of pH Interaction

The optimal pH for each solution of methylene blue and CBB by adjusting the pH was determined within the range of 3–12. Figure 5 displays the relationship between the pH of the adsorbate and the quantity of dye adsorbed ( $q_{exp}$ ). By observing Fig. 5a, it is evident that nAC-RFs-APTES adsorbs a higher amount of CBB and MB dyes compared to nAC-RFs. The optimal pH for the adsorption of CBB and MB dyes by nAC-RFs-APTES is pH 5 for both. The adsorption of CBB dye by nAC-RFs is significantly affected by the pH interaction, while the influence on the MB dye is relatively minimal.

The data regarding pH interaction effects are closely linked to the surface charge of the adsorbent, determined through pH<sub>pzc</sub> determination (Fig. 4). This study revealed that nAC-RFs-S has a pH<sub>pzc</sub> value of 9.02, while the optimal adsorption of CBB and MB takes place at pH 5. Under acidic conditions,

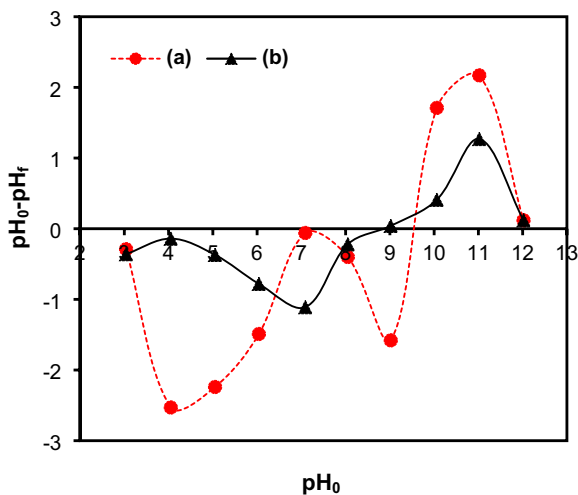


**Fig. 4** The pH<sub>pzc</sub> value curves of (a) nAC-RFs and (b) nAC-RFs-S

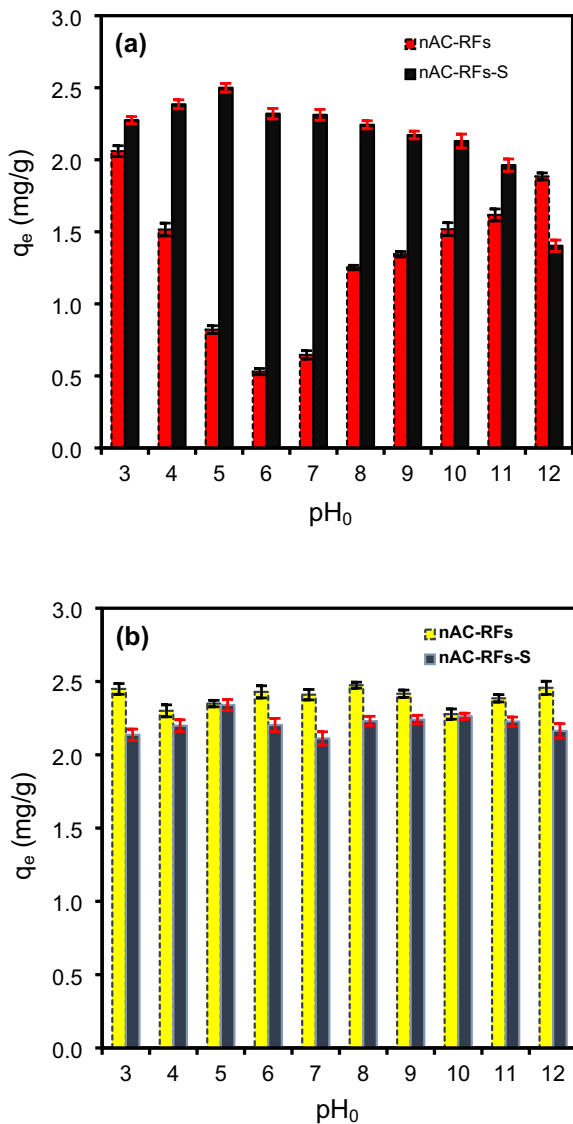


**Fig. 5** The influence of pH on dye adsorption of (a) CBB dan (b) MB by nAC-RFs dan nAC-RFs-S ( $C_0$ : 10 mg/L;  $V$ : 0.025 L;  $T$ :  $27 \pm 1$  °C;  $t$ : 60 min; Agitation Speed: 150 rpm; adsorbent mass: 0.1 g)

functional groups like hydroxyl and carboxylate on nAC-RFs, as well as amino groups from APTES on nAC-RFs-S, undergo significant protonation, resulting in a positive charge (An et al., 2020). Consequently, both adsorbents tend to possess a positive surface charge, leading to strong interactions with anionic adsorbates such as CBB, compared to cationic MB (Sharma et al., 2017). The anionic dye CBB is prone to adsorption under acidic conditions due

to electrostatic interactions with the  $H^+$ -rich surface of the adsorbent, yielding more favorable adsorption than under alkaline conditions. Moreover, at that specific pH, the interaction between MB and nAC-RFs and nAC-RFs-S is more likely to occur via cation exchange reactions since the positively charged surface of the adsorbent aligns with the positive charge of the MB dye. Furthermore, interactions can also occur within the pore cavities of the adsorbent (Buhani et al., 2023).

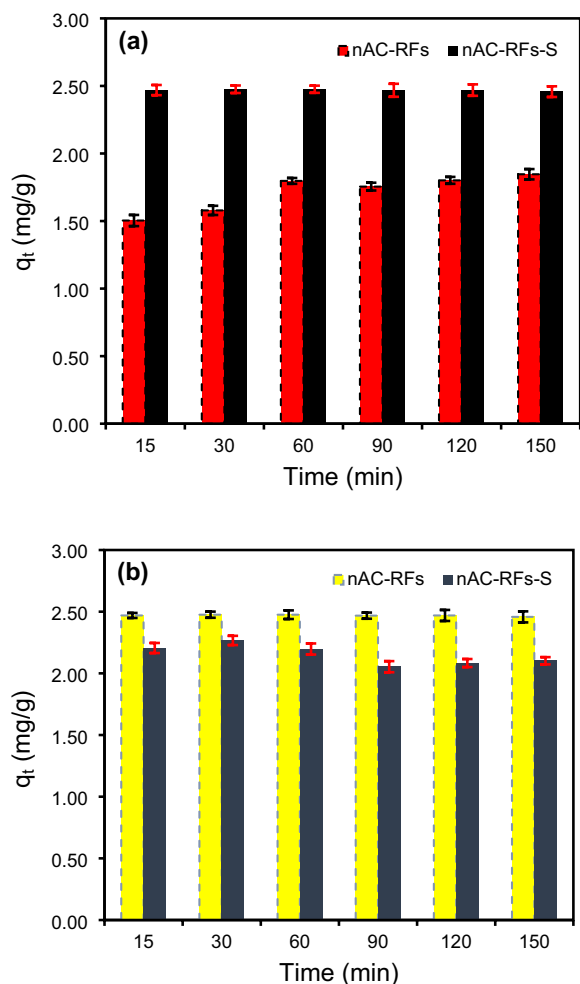
### 3.4 Effect of Interaction Time

Figure 6 illustrates how the duration of contact affects the adsorption of CBB and MB individually by nAC-RFs and nAC-RFs-S. This adsorption process involved varying contact times from 0 to 150 min. The quantity of CBB or MB adsorbed by the adsorbent ( $q_{exp}$ ) showed a relatively consistent increase after the initial 15 min until reaching a contact time of 150 min for nAC-RFs-S. This indicates that the adsorption equilibrium for both CBB and MB on the respective adsorbents is rapidly established. In Fig. 6a, it is evident that nAC-RFs-S exhibit higher adsorption of CBB compared to nAC-RFs. Conversely, in the case of MB adsorption (Fig. 6b), nAC-RFs demonstrate greater adsorption than nAC-RFs-S. This distinction can be attributed to the anionic nature of CBB, which favors interaction with a positively charged adsorbent surface. The presence of amino groups from the silane agent and hydroxyl groups on nAC-RFs results in a positively charged surface of the adsorbent at pH 5 due to protonation.

### 3.5 Adsorption Kinetics

The rate at which the dye is adsorbed is determined by examining how the duration of contact during adsorption affects the amount of dye that becomes adsorbed, as depicted in Fig. 6. The data in Fig. 6 were subjected to analysis using mathematical models, namely the pseudo-first-order kinetic model (Eq. 4) and the pseudo-second-order kinetic model (Eq. 5) (Ho & McKay, 1999), which are presented below:

$$\log(q_e - q_t) = \log q_e - \frac{k_1}{2.303} t \quad (4)$$



**Fig. 6** The influence of contact time on adsorption of (a) CBB and (b) MB by nAC-RFs and nAC-RFs-S ( $C_0$ : 10 mg/L;  $pH_0$ : 5.0;  $V$ : 0.025 L;  $T$ :  $27 \pm 1$  °C; agitation speed: 150 rpm; adsorbent mass: 0.1 g)

$$\frac{t}{q_t} = \frac{1}{k_2 q_e^2} + \frac{t}{q_e} \tag{5}$$

where  $q_t$  and  $q_e$  (mg/g) are total CBB or MB adsorption capacity at time  $t$  and equilibrium, respectively,  $k_1$

and  $k_2$  are the Pseudo-first order and Pseudo-second order rate constants, respectively. The parameters of adsorption kinetics, such as the adsorption rate constant and regression coefficients of CBB and MB on nAC-RFs and nAC-RFs-S, are presented in Table 1.

In the equations,  $q_t$  and  $q_e$  (mg/g) represent the total adsorption capacity of CBB or MB at time  $t$  and equilibrium, respectively. The rate constants  $k_1$  and  $k_2$  correspond to the first-order and second-order kinetics, respectively. Table 1 displays the kinetic parameters including the adsorption rate constant and regression coefficients for CBB and MB on nAC-RFs and nAC-RFs-S.

By examining Table 1, it becomes evident that the adsorption of CBB and MB dyes by nAC-RFs and nAC-RFs-S tends to adhere to the pseudo-second-order kinetic model. This can be deduced from the high correlation coefficient ( $R^2$ ) values of both dyes on each adsorbent, which are both 0.999. Such findings indicate that the pseudo-second-order kinetic model is more appropriate compared to the pseudo-first-order kinetic model. According to the pseudo-second-order kinetic model, the adsorption process of CBB and MB dyes onto nAC-RFs and nAC-RFs-S involves not only physical interactions but also chemical interactions with the active groups present on the adsorbent (Buhani et al., 2021a). Moreover, the characteristic data of the adsorption kinetics listed in Table 1 demonstrate that the pseudo-second-order adsorption rate constant ( $k_2$ ) for CBB on nAC-RFs-S surpasses that of nAC-RFs. Furthermore, the  $k_2$  value for MB is higher on nAC-RFs. These observations align with the earlier discussion regarding the influence of pH, which elucidates the compatibility between the charge characteristics of the adsorbate and the active sites of the adsorbent.

### 3.6 Adsorption Isotherms

The impact of the initial concentration ( $C_0$ ) on the adsorption of CBB and MB by nAC-RFs and nAC-RFs-S is

**Table 1** Characteristics of adsorption kinetics parameters for CBB and MB dyes by nAC-RFs and nAC-RFs-S ( $C_0$ : 10 mg/L;  $pH_0$ : 5.0;  $V$ : 0.025 L;  $T$ :  $27 \pm 1$  °C; Agitation Speed: 150 rpm; adsorbent mass: 0.1 g)

Adsorbents-Adsorbats	Pseudo-first-order		Pseudo-second-order		
	$k_1 \times 10^{-4}$ (1/min)	$R^2$	$q_e$ (mg/g)	$k_2 \times 10^{-3}$ (g/ mg. min)	$R^2$
nAC-RFs—CBB	8.00	0.462	3.450	0.185	0.999
nAC-RFs-S—CBB	3.00	0.277	5.843	2.674	0.999
nAC-RFs—MB	3.10	0.264	6.064	2.735	0.999
nAC-RFs-S -MB	1.10	0.620	2.076	0.415	0.999



evident in Fig. 7. Based on the data presented in Fig. 7, it is noticeable that the adsorbed amounts of CBB and MB increase as the  $C_0$  of each dye rises. The steep rise in  $q_{exp}$  at low  $C_0$ , followed by further increments at high  $C_0$ , signifies that nAC-RFs-S exhibits significantly higher adsorption affinity towards CBB in comparison to nAC-RFs. This enhanced adsorption can be attributed to the availability of active sites on the surface of the adsorbent (Atar et al., 2012). The presence of additional active adsorption sites in nAC-RFs-S, resulting from its modification with silane agents, contributes to this phenomenon. These supplementary active groups comprise amines, silanols, and siloxanes, in addition to the active sites already present in nAC-RFs, such as porous voids and hydroxyl groups.

In addition, to determine the suitable adsorption isotherm models for CBB and MB by nAC-RFs and nAC-RFs-S, the data analyzing the effect of initial adsorbate concentrations (CBB and MB) on the

adsorbed amount of adsorbate (Fig. 7a and b) were subjected to analysis using adsorption isotherm models. Two adsorption isotherm models, namely the Langmuir and Freundlich models, were employed in this research.

The Langmuir adsorption isotherm model explains that the adsorbent surface contains a specific number of active sites that are proportional to the surface area. Consequently, the adsorbent surface exhibits uniformity, and the adsorption process occurs in a monolayer manner, as represented by Eq. 6 (Álvarez-Torrellas et al., 2016; Buhani et al., 2021b).

$$\frac{1}{q_e} = \frac{1}{q_m K_L C_e} + \frac{1}{q_m} \tag{6}$$

In the given context,  $C_e$  (mg/L) represents the concentration of the dye solution at equilibrium,  $q_e$  (mg/g) denotes the adsorption capacity of the dye at equilibrium,  $q_m$  refers to the monolayer adsorption capacity of the adsorbent, and  $K_L$  represents the equilibrium constant that reflects the affinity of binding sites (L/mg). Parameters like  $K_L$  and  $q_m$  can be determined by plotting a linear equation of  $\log 1/q_e$  versus  $C_e$ , resulting in a straight line with a slope of  $1/q_m K_L$  and an intercept of  $1/q_m$ .

Additionally, the Freundlich isotherm model is an empirical equation employed for heterogeneous systems and adsorption at multiple layers (Shao et al., 2016). This model is expressed by Eq. 7.

$$\log q_e = \log K_F + \frac{1}{n} \log C_e \tag{7}$$

$K_F$  is the adsorption capacity factor, expressed in  $((\text{mg/g}) (\text{L/mg})^{1/n})$ , where  $n$  is the adsorption intensity factor ranging from 1 to 10 (Ho and McKay, 2001). The adsorption parameters, such as  $K_F$  and  $n$ , are obtained by plotting  $\log q_e$  against  $\log C_e$ .

Table 2 presents the analysis results of the adsorption parameters for CBB and MB by nAC-RFs and nAC-RFs-S using the Langmuir and Freundlich adsorption isotherm models.

Based on the data presented in Table 2, it can be observed that the adsorption behavior of CBB dye tends to align with the Freundlich adsorption isotherm model when using nAC-RFs, while it follows the Langmuir adsorption isotherm model when using nAC-RFs-S. Similarly, the adsorption of MB dye, for both nAC-RFs and nAC-RFs-S, tends to conform

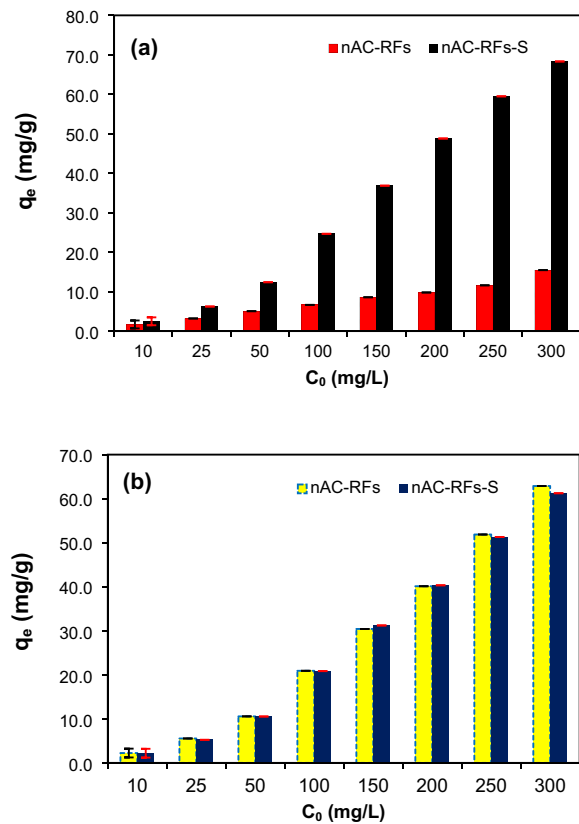


**Fig. 7** Influence of initial concentration on adsorption of (a) CBB and (b) MB dye onto nAC-RFs and nAC-RFs-S ( $C_0$ : 10–300 mg/L;  $\text{pH}_0$ : 5.0;  $V$ : 0.025 L;  $t$ : 90 min;  $T$ :  $27 \pm 1$  °C; agitation speed: 150 rpm; adsorbent mass: 0.1 g)

to the Freundlich adsorption isotherm model. These trends are evident from the  $R^2$  values obtained for each interaction between the adsorbent and adsorbate. The interaction between CBB and nAC-RFs-S exhibits characteristics consistent with the Langmuir adsorption isotherm model, indicating a dominant role of chemical interactions in the adsorption process. The presence of active groups, such as hydroxyl, amine, and carboxyl groups (Fig. 2), in nAC-RFs-S originates from both nAC-RFs and the APTES modifying agent.

Moreover, the adsorption of MB by both nAC-RFs and nAC-RFs-S also tends to follow the Freundlich adsorption isotherm model, as observed in the interaction between CBB and nAC-RFs. This suggests that the adsorption process is primarily governed by physical interactions, including pore cavities and ion exchange. The relatively smaller size of MB molecules compared to CCB contributes to their enhanced adsorption through the pore cavities of both nAC-RFs and nAC-RFs-S. This observation is supported by higher  $K_F$  and  $n$  values in the nAC-RFs-MB interaction compared to nAC-RFs-S-MB. Specifically, the  $K_F$  values are 2.132 and 1.669 (mg/g) (L/mg)<sup>1/n</sup> for nAC-RFs and nAC-RFs-S, respectively, while the  $n$  values are 1.207 and 1.103, respectively. The suitability of the  $n$  value in adsorption can be categorized as very good if it falls within the range of 2 to 10, satisfactory if it ranges from 1 to 2, and poor if it is below 1 (Liang et al., 2017).

### 3.7 The Influence of Similar Ions

The CBB dye, which has an anionic nature, exhibits its strong adsorption affinity towards nAC-RFs-S. Consequently, the impact of similar ions was investigated by conducting adsorption competition experiments using nitrate and phosphate anions at concentrations of 0.1, 0.25, and 0.35 mmol/L on nAC-RFs-S. The findings of the adsorption competition are presented in Fig. 8. Analysis of the data

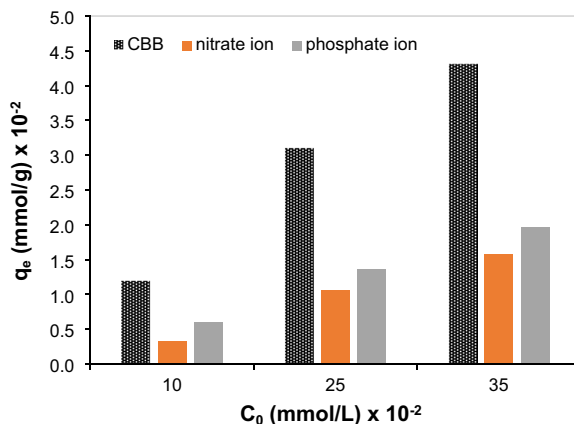


**Fig. 8** The influence of similar ions (nitrate and phosphate anions) on the amount of CBB adsorbed by nAC-RFs-S

in Fig. 8 reveals that across all three concentrations tested on nAC-RFs-S, the CBB dye is significantly more adsorbed compared to nitrate and phosphate ions. This outcome demonstrates the superior selectivity of nAC-RFs-S towards CBB. The presence of aromatic groups in the CBB molecule enhances the stability of the negative charge on its functional groups, thereby influencing the electrostatic interactions and  $\pi$ - $\pi$  bonding between the adsorbent and the adsorbate (Yilmaz, 2022).

### 3.8 The Ability of Reusability

The reusability of nAC-RFs-S as an adsorbent for CBB and MB is a crucial parameter for assessing the quality of the adsorbent. The purpose of reusing the adsorbent in multiple adsorption cycles is to maximize its effectiveness. Desorption of CBB and MB is carried out using a 40% ethanol eluent, which effectively removes the dyes from nAC-RFs-S by leveraging both physical and chemical interactions (such as electrostatic or cation exchange interactions) due to the polar nature

**Table 2** Langmuir and Freundlich parameters for the adsorption of CBB and MB dyes by nAC-RFs and nAC-RFs-S ( $C_0$ : 10 mg/L;  $pH_0$ : 5.0;  $V$ : 0.025 L;  $t$ : 90 min;  $T$ :  $27 \pm 1$  °C; agitations speed: 150 rpm; adsorbent mass: 0.1 g)

Adsorbent-adsorbate	$q_{exp}$ (mg/g)	Langmuir			Freundlich		
		$q_m$ (mg/g)	$K_L$ (L/mg)	$R^2$	$K_F$ (mg/g). (L/mg) <sup>1/n</sup>	$n$	$R^2$
nAC-RFs - CBB	15.449	14.582	0.182	0.865	1.066	2.110	0.984
nAC-RFs-S - CBB	68.317	73.113	4.468	0.989	17.239	1.897	0.930
nAC-RFs - MB	62.870	28.558	0.026	0.510	2.132	1.207	0.992
nAC-RFs-S -MB	61.233	34.392	0.018	0.430	1.669	1.103	0.993

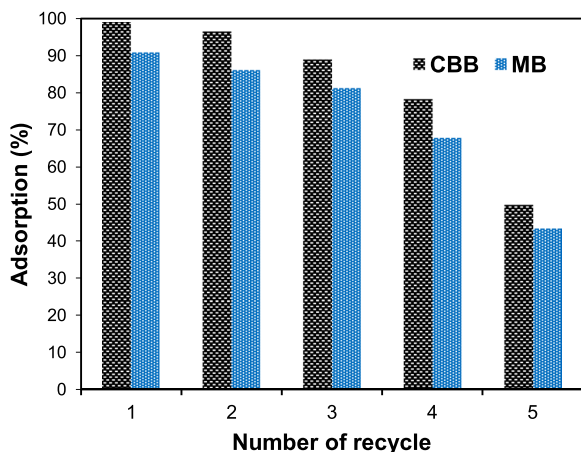


**Fig. 9** The reuse of nAC-RFs-S for CBB and MB adsorption

of the solution. Figure 9 demonstrates that nAC-RFs-S can be reused for up to three cycles, with over 80% of the initially adsorbed CBB and MB still being desorbed. However, in the fourth adsorption cycle, there is a decrease in the amount of CBB and MB adsorbed, with percentages of 78.08 and 67.75%, respectively. This decline can be attributed to the desorption process and the neutralization of the adsorbent, which may impair the active sites of nAC-RFs-S (Buhani et al., 2023). Therefore, it can be concluded that nAC-RFs-S is an effective adsorbent that exhibits efficient adsorption of CBB and MB dyes and can be reused.

#### 4 Conclusion

The modification of non-activated carbon derived from rubber fruit shells through APTES has successfully yielded the nAC-RFs-S adsorbent. The adsorption behavior of CBB on nAC-RFs-S tends to align with the Langmuir adsorption isotherm model, whereas MB conforms to the Freundlich adsorption isotherm model. The desorption of both CBB and MB from nAC-RFs-S can be easily achieved using polar solvents such as a 40% ethanol solution. The nAC-RFs-S adsorbent exhibits reusability in adsorption–desorption cycles for up to three repetitions, with CBB and MB displaying adsorption percentages exceeding 80%. With its substantial capacity and strong affinity towards anionic CBB and cationic MB dyes, nAC-RFs-S serves as an effective solution for mitigating water pollution caused by toxic synthetic dyes, irrespective of their cationic or anionic properties.

**Acknowledgements** The authors express their gratitude to the Ministry of Education, Culture, Research, and Technology of the Republic of Indonesia (KemendikbudRistek) for providing funding for this project under contract number: 027/E5/PG.02.00.PL/2023. We also acknowledge the support of the Research and Community Service Institute of the University of Lampung (LPPM Universitas Lampung) for their assistance in conducting this research.

**Author Contribution** **Buhani:** Conceptualization, methodology, Investigation, Data curation, and writing original draft.

**Jilda Sofiana Dewi:** Methodology, Investigation, and Data curation.

**Nadya Syarifatul Fajriyah:** Methodology, Investigation, and Data curation.

**Mita Rilyanti:** Methodology, Investigation, Data curation, and Data analysis.

**Suharso:** Conceptualization, methodology, Investigation, and Data curation.

**Sumadi:** Conceptualization, Data curation, Data analysis, and editing.

**Khalid Z. Elwakeel:** Review and editing.

**Funding** This work was funded by Ministry of Education, Culture, Research and Technology (Kemdikbudristek) of the Republic of Indonesia with contract number: 027/E5/PG.02.00.PL/2023.

**Data Availability** All data generated or analyzed during this study are included in this published article.

#### Declarations

**Ethics Approval** Not applicable.

**Consent to Participate** Not applicable.

**Consent for Publication** Not applicable.

**Competing Interests** The authors declare no competing interests.

#### References

- Abdel-Ghani, N. T., El-Chaghaby, G. A., Rawash, E. S. A., & Lima, E. C. (2017). Adsorption of coomassie brilliant blue r-250 dye onto novel activated carbon prepared from nigella sativa l. waste: equilibrium, kinetics and thermodynamics running title: adsorption of brilliant blue dye onto *Nigella sativa* L. waste activated carbon. *Journal of the Chilean Chemical Society*, 62(2), 3505–3511. <https://doi.org/10.4067/S0717-97072017000200016>
- Ahmad, A., Razali, M. H., Mamat, M., Mehamod, F. S. B., & Amin, K. A. M. (2017). Adsorption of methyl orange by synthesized and functionalized-CNTs with 3-Aminopropyltriethoxysilane loaded TiO<sub>2</sub> nanocomposites.

- Chemosphere*, 168, 474–482. <https://doi.org/10.1016/j.chemosphere.2016.11.028>
- Ai, L., Zhang, C., Liao, F., Wang, Y., Li, M., Meng, L., & Jiang, J. (2011). Removal of methylene blue from aqueous solution with magnetite loaded multi-wall carbon nanotube: Kinetic, isotherm and mechanism analysis. *Journal of Hazardous Materials*, 198, 282–290. <https://doi.org/10.1016/j.jhazmat.2011.10.041>
- Al-Hazmi, G. H., Akhdhar, A., Shahat, A., & Elwakeel, K. Z. (2022). Adsorption of gentian violet dye onto mesoporous aluminosilica monoliths: Nanoarchitectonics and application to industrial wastewater. *International Journal of Environmental Analytical Chemistry*. <https://doi.org/10.1080/03067319.2022.2104641>
- Álvarez-Torrellas, S., Muñoz, M., Zazo, J. A., Casas, J. A., & García, J. (2016). Synthesis of high surface area carbon adsorbents prepared from pine sawdust-Onopordum acanthium L. for nonsteroidal antiinflammatory drugs adsorption. *Journal of Environmental Management*, 183, 294–305. <https://doi.org/10.1016/j.jenvman.2016.08.077>
- An, L., Si, C., Bae, J. H., Jeong, H., & Kim, Y. S. (2020). One-step silanization and amination of lignin and its adsorption of Congo red and Cu(II) ions in aqueous solution. *International Journal of Biological Macromolecules*, 159(2020), 222–230. <https://doi.org/10.1016/j.ijbiomac.2020.05.072>
- Atar, N., Olgun, A., & Wang, S. (2012). Adsorption of cadmium (II) and zinc (II) on boron enrichment process waste in aqueous solutions: Batch and fixed-bed system studies. *Chemical Engineering Journal*, 192(3), 1–7. <https://doi.org/10.1016/j.cej.2012.03.067>
- Bhavyasree, P. G., & Xavier, T. S. (2021). Adsorption studies of methylene blue, coomassie brilliant blue, and congo red dyes onto CuO/C nanocomposites synthesized via vitex negundo linn leaf extract. *Current Research in Green and Sustainable Chemistry*, 4, 100161. <https://doi.org/10.1016/j.crgsc.2021.100161>
- Buhani, Rinawati, Suharso, Yuliasari, D. P., & Yuwono, S. D. (2017). Removal of Ni(II), Cu(II), and Zn(II) ions from aqueous solution using *Tetraselmis* sp. biomass modified with silica-coated magnetite nanoparticles. *Desalination and Water Treatment*, 80, 203–213. <https://doi.org/10.5004/dwt.2017.20932>
- Buhani, Hariyanti, F., Suharso, Rinawati, & Sumadi. (2019). Magnetized algae-silica hybrid from porphyridium sp. biomass with Fe<sub>3</sub>O<sub>4</sub> particle and its application as adsorbent for the removal of methylene blue from aqueous solution. *Desalination and Water Treatment*, 142, 331–340. <https://doi.org/10.5004/dwt.2019.23533>
- Buhani, S., Rilyanti, M., Sari, M., & Sumadi. (2021a). Removal of Cd(II) ions in solution by activated carbon from palm oil shells modified with magnetite. *Desalination and Water Treatment*, 218, 352–362. <https://doi.org/10.5004/dwt.2021.26978>
- Buhani, Wijayanti, T. A., Suharso, Sumadi, & Ansori, M. (2021b). Application of modified green algae *Nannochloropsis* sp. as adsorbent in the simultaneous adsorption of methylene blue and Cu(II) cations in solution. *Sustainable Environment Research*, 31(17), 1–12. <https://doi.org/10.1186/s42834-021-00090-y>
- Buhani, S., Rilyanti, M., Devi, F., Antika, R., Puji, L., & Sumadi, L. (2023). Functionalization of carbon from rubber fruit shells (*Hevea brasiliensis*) with silane agents and its application to the adsorption of bi-component mixtures of methylene blue and crystal violet. *Environmental Science and Pollution Research*. <https://doi.org/10.1007/s11356-023-28031-9>
- Can, K., Ozmen, M., & Ersoz, M. (2009). Immobilization of albumin on aminosilane modified superparamagnetic magnetite nanoparticles and its characterization. *Colloids and Surfaces B: Biointerfaces*, 71(1), 154–159. <https://doi.org/10.1016/j.colsurfb.2009.01.021>
- Çelekli, A., & Bozkurt, H. (2013). Predictive modeling of an azo metal complex dye sorption by pumpkin husk. *Environmental Science and Pollution Research*, 20(10), 7355–7366. <https://doi.org/10.1007/s11356-013-1751-5>
- Elgarahy, A. M., Elwakeel, K. Z., Elshoubaky, G. A., & Mohammad, S. H. (2019). Untapped sepia shell-based composite for the sorption of cationic and anionic dyes. *Water, Air, & Soil Pollution*, 230, 217. <https://doi.org/10.1007/s11270-019-4247-1>
- Elgarahy, A. M., Elwakeel, K. Z., Mohammad, S. H., & Elshoubaky, G. A. (2021). A critical review of biosorption of dyes, heavy metals and metalloids from wastewater as an efficient and green process. *Cleaner Engineering and Technology*, 4, 100209. <https://doi.org/10.1016/j.clet.2021.100209>
- Elwakeel, K. Z., Shahat, A., Khan, Z. A., Alshitari, W., & Guibal, E. (2020). Magnetic metal oxide-organic framework material for ultrasonic-assisted sorption of titan yellow and rose bengal from aqueous solutions. *Chemical Engineering Journal*, 392, 123635. <https://doi.org/10.1016/j.cej.2019.123635>
- Fajriyah, N. S., Buhani, B., & Suharso, S. (2023). Adsorption kinetics and isotherm of crystal violet by carbon modified with magnetite (Fe<sub>3</sub>O<sub>4</sub>) and triethoxyphenylsilane (TEPS) from rubber fruit shell. *Indonesian Journal of Chemistry*, 23(1), 170–183. <https://doi.org/10.22146/ijc.76201>
- Ho, Y. S., & McKay, G. (1999). Pseudo-second order model for sorption processes. *Process Biochem*, 34(5), 451–465. [https://doi.org/10.1016/S0032-592\(98\)00112-5](https://doi.org/10.1016/S0032-592(98)00112-5)
- Huang, C., & Hu, B. (2008). Silica-coated magnetic nanoparticles modified with  $\gamma$ -Mercaptopropyltrimethoxysilane for fast and selective solid phase extraction of trace amounts of Cd, Cu, Hg, and Pb in environmental and biological samples prior to their determination by inductively Co. *Spectrochimica Acta - Part B Atomic Spectroscopy*, 63(3), 437–444. <https://doi.org/10.1016/j.sab.2007.12.010>
- Ibrahim, H. K., Al-Da' Amy, M. A., & Kreem, E. T. (2019). Decolorization of coomassie brilliant blue G-250 dye using snail shell powder by action of adsorption processes. *Research Journal of Pharmacy and Technology*, 12(10), 4921–4925. <https://doi.org/10.5958/0974-360X.2019.00853.9>
- Iwuozor, K. O., Ighalo, J. O., Ogunfowora, L. A., Adeniyi, A. G., & Igwegbe, C. A. (2021). An empirical literature analysis of adsorbent performance for methylene blue uptake from aqueous media. *Journal of Environmental Chemical Engineering*, 9(4), 105658. <https://doi.org/10.1016/j.jece.2021.105658>
- Jamwal, H. S., Kumari, S., Chauhan, G. S., Reddy, N. S., & Ahn, J. H. (2017). Silica-polymer hybrid materials as methylene blue adsorbents. *Journal of Environmental*

- Chemical Engineering*, 5(1), 103–113. <https://doi.org/10.1016/j.jece.2016.11.029>
- Kanakaraju, D., Ravichandar, S., & Lim, Y. C. (2017). Combined effects of adsorption and photocatalysis by hybrid TiO<sub>2</sub>/ZnO-calcium alginate beads for the removal of copper. *Journal of Environmental Sciences (China)*, 55, 214–223. <https://doi.org/10.1016/j.jes.2016.05.043>
- Katheresan, V., Kansedo, J., & Lau, S. Y. (2018). Efficiency of various recent wastewater dye removal methods: A review. *Journal of Environmental Chemical Engineering*, 6(4), 4676–4697. <https://doi.org/10.1016/j.jece.2018.06.060>
- Kosa, S. A., Al-Zhrani, G., & Abdel Salam, M. (2012). Removal of heavy metals from aqueous solutions by multi-walled carbon nanotubes modified with 8-Hydroxyquinoline. *Chemical Engineering Journal*, 181–182, 159–168. <https://doi.org/10.1016/j.cej.2011.11.044>
- Lee, S., Jeong, J., Shin, S., Kim, J. C., & Kim, J. D. (2004). Synthesis and characterization of superparamagnetic maghemite nanoparticles prepared by coprecipitation technique. *Journal of Magnetism and Magnetic Materials*, 282, 147–150. <https://doi.org/10.1016/j.jmmm.2004.04.035>
- Liang, X., Lu, Y., Li, Z., Yang, C., Niu, C., & Su, X. (2017). Bentonite/carbon composite as highly recyclable adsorbents for alkaline wastewater treatment and organic dye removal. *Microporous and Mesoporous Materials*, 241, 107–114. <https://doi.org/10.1016/j.micromeso.2016.12.016>
- Liu, Y., Li, Y., Li, X. M., & He, T. (2013). Kinetics of (3-Aminopropyl)triethoxysilane (APTES) silanization of superparamagnetic iron oxide nanoparticles. *Langmuir*, 29(49), 15275–15282. <https://doi.org/10.1021/la403269u>
- Moosavi, S., Lai, C. W., Gan, S., Zamiri, G., Akbarzadeh Pivezhani, O., & Johan, M. R. (2020). Application of efficient magnetic particles and activated carbon for dye removal from wastewater. *ACS Omega*, 5(33), 20684–20697. <https://doi.org/10.1021/acsomega.0c01905>
- Munguía-Cortés, L., Pérez-Hermosillo, I., Ojeda-López, R., Esparza-Schulz, J. M., Felipe-Mendoza, C., Cervantes-Urbe, A., & Domínguez-Ortiz, A. (2017). APTES-functionalization of SBA-15 using ethanol or toluene: Textural characterization and sorption performance of carbon dioxide. *Journal of the Mexican Chemical Society*, 61(4), 273–281. <https://doi.org/10.29356/jmcs.v61i4.457>
- Priya, Kaith, B. S., Shanker, U., Gupta, B., & Bhatia, J. K. (2018). RSM-CCD optimized in-air synthesis of photocatalytic nanocomposite: Application in removal-degradation of toxic brilliant blue. *Reactive and Functional Polymers*, 131(107), 122. <https://doi.org/10.1016/j.reactfunctpolym.2018.07.016>
- Radoičić, M., Šaponjić, Z., Nedeljković, J., Ćirić-Marjanović, G., & Stejskal, J. (2010). Self-assembled polyaniline nanotubes and nanoribbons/titanium dioxide nanocomposites. *Synthetic Metals*, 160(11–12), 1325–1334. <https://doi.org/10.1016/j.synthmet.2010.04.010>
- Rocha, L. S., Pereira, D., Sousa, É., Otero, M., Esteves, V. I., & Calisto, V. (2020). Recent advances on the development and application of magnetic activated carbon and char for the removal of pharmaceutical compounds from waters: A review. *Science of the Total Environment*, 718, 137272. <https://doi.org/10.1016/j.scitotenv.2020.137272>
- Sahoo, S. K., Panigrahi, G. K., Sahoo, J. K., Pradhan, A. K., Purohit, A. K., & Dhal, J. P. (2021). Electrospun magnetic polyacrylonitrile-GO hybrid nanofibers for removing Cr(VI) from water. *Journal of Molecular Liquids*, 326, 115364. <https://doi.org/10.1016/j.molliq.2021.115364>
- Shao, Y., Zhou, L., Bao, C., Ma, J., Liu, M., & Wang, F. (2016). Magnetic responsive metal–organic frameworks nanosphere with core–shell structure for highly efficient removal of methylene blue. *Chemical Engineering Journal*, 283, 1127–1136. <https://doi.org/10.1016/j.cej.2015.08.051>
- Sharma, G., Naushad, M., Kumar, A., Rana, S., Sharma, S., Bhatnagar, A., Stadler, F. J., Ghfar, A. A., & Khan, M. R. (2017). Efficient removal of coomassie brilliant blue R-250 dye using starch/poly(alginate-chitosan) nanohydrogel. *Process Safety and Environmental Protection*, 109, 301–310. <https://doi.org/10.1016/j.psep.2017.04.011>
- Thamer, B. M., Aldalbah, A., Moydeen, A. M., El-Hamshary, H., Al-Enizi, A. M., & El-Newehy, M. H. (2019). Effective adsorption of coomassie brilliant blue dye using poly(phenylene diamine)grafted electrospun carbon nanofibers as a novel adsorbent. *Materials Chemistry and Physics*, 234(133), 145. <https://doi.org/10.1016/j.matchemphys.2019.05.087>
- Wong, K. T., Yoon, Y., & Jang, M. (2015). Enhanced recyclable magnetized palm shell waste-based powdered activated carbon for the removal of ibuprofen: Insights for kinetics and mechanisms. *PLoS One*, 10(10), 1–18. <https://doi.org/10.1371/journal.pone.0141013>
- Wong, K. T., Yoon, Y., Snyder, S. A., & Jang, M. (2016). Phenyl-functionalized magnetic palm-based powdered activated carbon for the effective removal of selected pharmaceutical and endocrine-disruptive compounds. *Chemosphere*, 152, 71–80. <https://doi.org/10.1016/j.chemosphere.2016.02.090>
- Yilmaz, M. S. (2022). Graphene oxide/hollow mesoporous silica composite for selective adsorption of methylene blue. *Microporous Mesoporous Mater*, 330, 111570. <https://doi.org/10.1016/j.micromeso.2021.111570>
- Zulaicha, A. S., Saputra, I. S., Buhani, B., & Suharsa, S. (2022). Magnetite particle coating to activated carbon of oil palm shells as adsorbent of Cu(II) and Ni(II) cation. *Journal of the Iranian Chemical Society*, 19(12), 4777–4787. <https://doi.org/10.1007/s13738-022-02641-5>

**Publisher's Note** Springer Nature remains neutral with regard to jurisdictional claims in published maps and institutional affiliations.

Springer Nature or its licensor (e.g. a society or other partner) holds exclusive rights to this article under a publishing agreement with the author(s) or other rightsholder(s); author self-archiving of the accepted manuscript version of this article is solely governed by the terms of such publishing agreement and applicable law.